Earth-Abundant Molecular Z-Scheme Photoelectrochemical Cell for Overall Water-Splitting

Christopher D. Windle, Hiromu Kumagai, Masanobu Higashi, Romain Brisse, Sébastien Bold, Bruno Jousselme, Murielle Chavarot-Kerlidou, Kazuhiko Maeda, Ryu Abe, Osamu Ishitani, et al.

Earth-Abundant Molecular Z-Scheme Photoelectrochemical Cell for Overall Water-Splitting

Christopher D. Windle,[1] Hiromu Kumagai,[2] Masanobu Higashi,[3] Romain Brisse,[4] Sebastian Bold,[1,5,6] Bruno Jousselme,[4] Murielle Chavarot-Kerlidou,[1] Kazuhiko Maeda,[2] Ryu Abe,[3*] Osamu Ishitani,[2*] Vincent Artero[*1]

[1]Laboratoire de Chimie et Biologie des Métaux, Université Grenoble Alpes, CNRS UMR 5249, CEA, 17 rue des Martyrs, F-38054 Grenoble, Cedex, France

[2]Department of Chemistry, School of Science, Tokyo Institute of Technology, O-okayama 2-12-1-NE-1, Meguro-ku, Tokyo 152-8550, Japan

[3]Department of Energy and Hydrocarbon Chemistry, Graduate School of Engineering, Kyoto University, Katsura, Nishikyo-ku, Kyoto 615-8510, Japan

[4]Laboratory of Innovation in Surface Chemistry and Nanosciences (LICSEN), NIMBE, CEA, CNRS, Université Paris-Saclay, CEA Saclay, 91191 Gif-sur-Yvette, Cedex, France
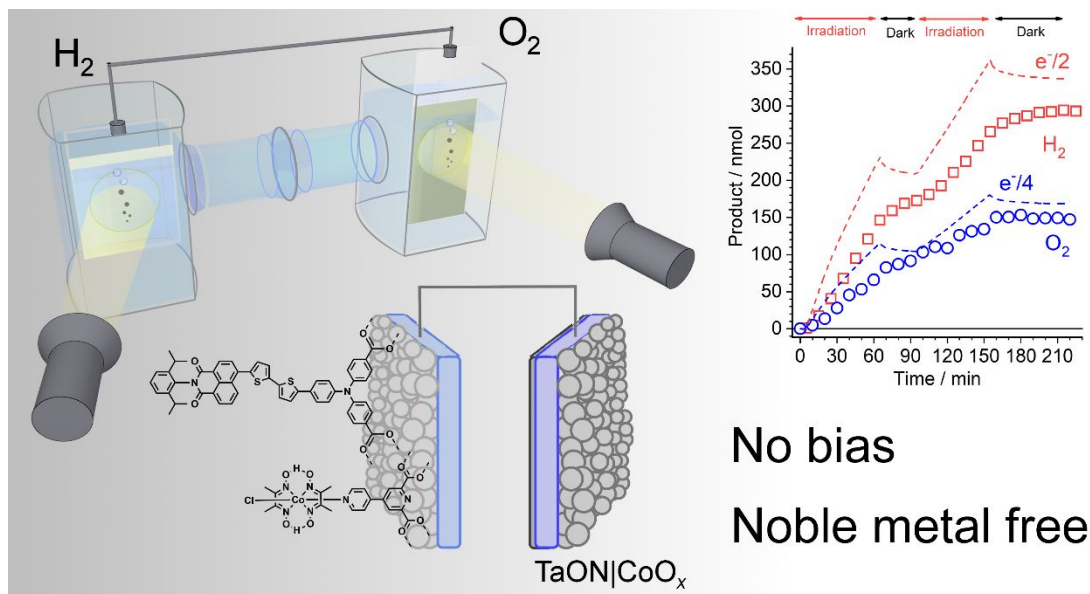
[5]Institute of Physical Chemistry and Abbe Center of Photonics, Friedrich Schiller University Jena, Helmholtzweg 4, 07743 Jena, Germany.

[6]Department Functional Interfaces, Leibniz Institute of Photonic Technology Jena (IPHT), Albert-Einstein-Straße 9, 07745 Jena, Germany.

ABSTRACT

A push-pull organic dye and a cobaloxime catalyst were successfully co-grafted on NiO and $CuGaO_2$ to form efficient molecular photocathodes for H_2 production with >80% Faradaic efficiency. $CuGaO_2$ is emerging as a more effective p-type semiconductor in photoelectrochemical cells and yields a photocathode with four-fold higher photocurrent densities and 400 mV more positive onset photocurrent potential compared to the one based on NiO. Such an optimized $CuGaO_2$ photocathode was combined with a TaON|CoO_x photoanode in a photoelectrochemical cell. Operated in this Z-scheme configuration, the two photoelectrodes produced H_2 and O_2 from

water with 87% and 88% Faradaic efficiency, respectively, at pH 7 under visible light and in the absence of an applied bias, equating to a solar to hydrogen conversion efficiency of 5.4×10^{-3}%. This is, to the best of our knowledge, the highest efficiency reported so far for a molecular-based noble metal-free water splitting Z-scheme.

INTRODUCTION

Hydrogen as an energy carrier is a promising alternative to fossil fuels because H_2 oxidation is pollution-free and allows for the closed-cycle storage and utilization of renewable energy. Splitting water into hydrogen and oxygen with the energy of sunlight is a potential sustainable source of hydrogen. Photoelectrochemical cells (PECs) can achieve such an artificial photosynthetic process. They are composed of photoelectrodes with built-in light absorbing layers that allow for electrochemical reactions to be driven directly by sunlight,[1] typically in a tandem configuration with a photocathode and a photoanode combined in circuit so that the photovoltages add to provide sufficient voltage to drive water splitting. Such a configuration mimics the Z-scheme found in photosynthetic organisms with photosystems I and II providing enough electrochemical potential across the thylakoid membrane to split water and produce reducing equivalents stored in NAD(P)H. In addition, the two photoelectrodes may absorb different regions of the visible spectrum and each photoelectrode performs one half-reaction of water splitting, thus the requirements of each component are reduced compared with using a single photocatalyst. The system can thus make more efficient use of the visible spectrum, leading to a higher theoretical limit on the efficiency.[2]

Among others,[3] a Z-scheme PEC cell was reported composed of a $Cu_2O|RuO_x$ photocathode and $BiVO_4|Mo$ photoanode, which could perform unassisted water splitting with 3% solar to hydrogen conversion efficiency (STH).[4]

Compared to photoanodes, photocathodes are much less developed. These include III-V semiconductors,[5] p-silicon,[5-6] metal oxides[5] and dye-sensitized transparent conducting oxides (DS-TCO).[7] III-V, silicon and metal oxide photocathodes generally exhibit relatively negative photocurrent onset potentials, which in an unbiased system, must be provided by the photoanode. It is also difficult to tune the materials toward desired absorption spectra and redox potentials. III-V photovoltaics are expensive and due to poor stability in aqueous conditions, involve an additional cost for protection layers, a case that also holds for silicon. DS-TCO based systems[8-18] operate in aqueous environments without protection layers and can be low-cost due to cheap TCO substrates and simple dyeing procedures.[19] The molecular components can be designed and synthesised with atomic precision, which allows precise tuning of the absorption spectrum and redox potentials. Molecular catalysts generally show good selectivity, which is important in the presence of oxygen.[20-21] DS-TCOs show promise as components for unbiased PEC cells for solar fuel production.[22-23] However, there are very few reports of unbiased DS-TCO Z-scheme water splitting cells, the most efficient reported so far produced H_2 with 55% Faradaic efficiency and a steady-state photocurrent of approximately 15 $\mu A\ cm^{-2}$ ($\lambda > 400$ nm, LED, 100 $mW.cm^{-2}$).[24-25] The system was reliant on ruthenium, which in the long term may not be cost-effective for scale up. Another report utilized a DS-TCO for CO_2 reduction within an unbiased PEC cell.[26]

DS-TCO photoelectrodes contain subcomponents for light absorption (dye), charge separation (p-type semiconductor) and catalysis (hydrogen evolution catalyst). Here, we present novel hybrid photocathodes constructed from a molecular dye (**RBG-174**) and a molecular catalyst (**CoHEC**) on p-type NiO (**Figure 1**) or $CuGaO_2$, an emerging alternative p-type material.[26] They proved active for hydrogen evolution and show enhanced performance when the NiO is replaced with $CuGaO_2$. This allowed the assembly of the most efficient noble metal-free Z-scheme molecular PEC cell for self-sustained water splitting reported so far, via coupling the $CuGaO_2$-based dye-sensitized photocathode with a **TaON|CoO$_x$** photoanode.

Results

Preparation and characterization of dye-sensitized photocathodes

The organic dye, **RBG-174**,[19] is based on a triphenylamine donor unit and a naphthalene monoimide acceptor, separated by a bridge of two thiophene groups (Figure 1). The dye has several intense absorption bands within the solar spectrum and a Dye/Dye$^-$ energy level of -1.68 V vs Fc$^+$/Fc.[27] **CoHEC** is a cobaloxime catalyst (Figure 1) with a trifunctional anchoring group.[28] This complex was analysed by cyclic voltammetry in dry DMF (Figure S1A) where it displayed an irreversible reduction at -1.1 V vs Fc$^{+/0}$ assigned to the reduction of Co^{III} into Co^{II} accompanied by release of the chloride anion.[29] A second reduction can be observed at -1.4 V vs Fc$^{+/0}$ assignable to the Co$^{II/I}$ couple. The addition of (Et$_3$NH)BF$_4$ as a proton source (Figure S1B) showed catalytic onset at the second reduction. Cyclic voltammetry in 2-(*N*-morpholino)ethanesulfonic acid (MES) buffer at pH 5.5 (Figure S2A) displayed an irreversible reduction at 0.12 V vs RHE and a catalytic onset for H$_2$ evolution at -0.24 V vs RHE corresponding to a low 240 mV overpotential requirement. The same overpotential was observed for **CoHEC** in pH 7 sodium phosphate buffer (Figure S2B). This operating potential is approximately 500 mV less negative than the potential of the **RBG-174/RBG-174$^-$** couple (Table S1), highlighting the significant driving force for electron transfer from the reduced dye to produce the active state of the catalyst. To prepare the NiO films we elaborated on established methods to produce a film 750 nm thick (Figure S3)[10] and used ozone treatment to increase the performance.[30]

The NiO films were then sensitized with **RBG-174** and functionalized with **CoHEC** (see the experimental section). The resulting **NiO|RBG-174|CoHEC** electrode was characterized by UV/Vis spectroscopy, inductively coupled plasma atomic emission spectroscopy (ICP-AES) and X-ray photoelectron spectroscopy (XPS). The UV/Vis spectrum (Figure S4) was taken in NaCl (0.1 M) with the electrode poised at 0 V vs Ag/AgCl to maximize the transparency of the NiO.[31] It shows a strong absorption with a maximum at 353 nm indicating a slight blue-shift compared with the measurement in CH$_2$Cl$_2$ solution.[9] Taking the molar absorption co-efficient as measured in CH$_2$Cl$_2$[9] a surface coverage of 19 nmol cm^{-2} (geometrical area) can be estimated. ICP-AES measurements of Co (see Experimental Section for sample preparation) showed a surface coverage of 12 nmol cm^{-2} of geometrical area. The dye and catalysts are therefore present at similar surface concentrations on the NiO substrate. X-ray photoelectron spectroscopy (XPS) confirmed the presence of cobalt(III) at the pristine electrode (Figure S5), in good agreement with data reported for related cobalt diimine-dioxime complexes grafted on ITO, NiO or MWCNT.[9, 32-33]
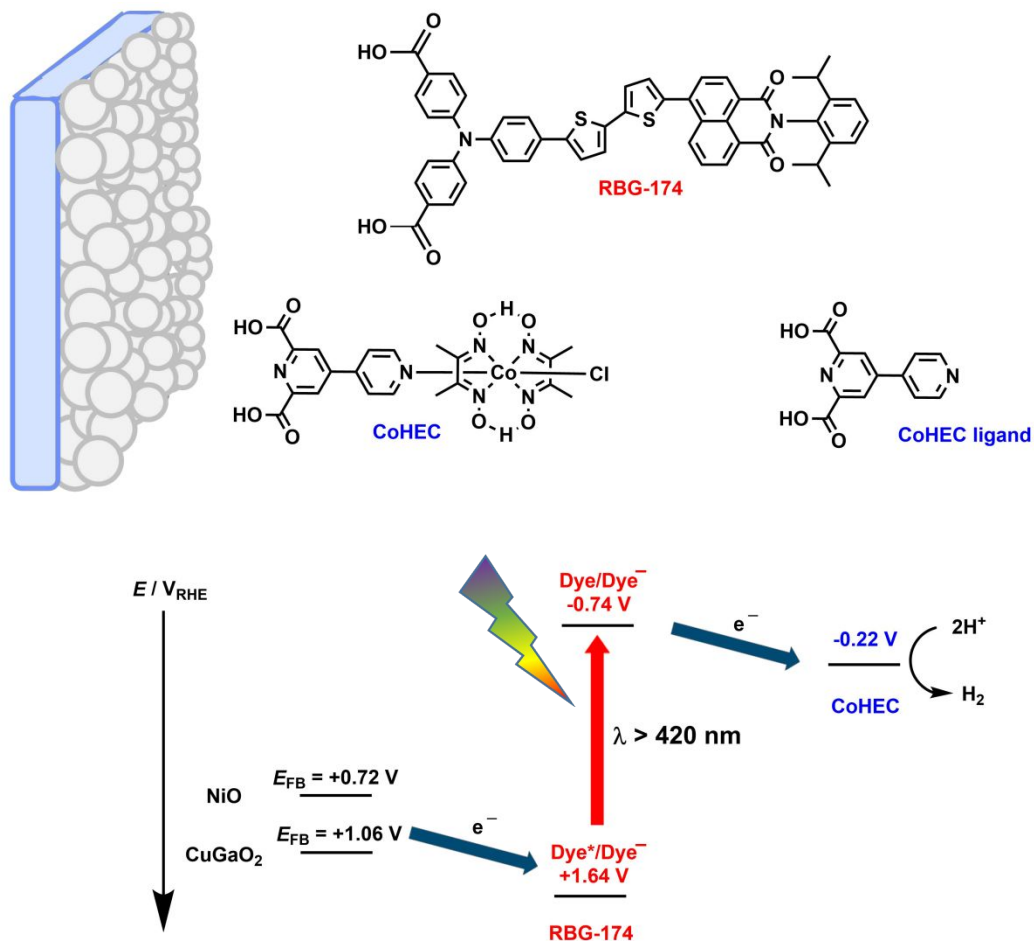
Figure 1. Molecular structures and energy diagram) of the photocathode. **CoHEC** redox potential is the onset of catalysis at pH 7. Electrochemical potentials given vs RHE, flat band position of NiO corrected from V vs NHE (pH 7) and flat band position of CuGaO$_2$ corrected from V vs Ag/AgCl (pH 6.6).[26, 34]

The **NiO|RBG-174|CoHEC** electrode was analysed by linear sweep voltammetry (LSV) (MES buffer, 0.1 M, pH 5.5). MES buffer was initially selected as we have shown this to be a suitable medium for photoelectrodes based on cobaloxime derivatives and organic dyes.[9-10, 35] Scanning from to 0.75 to −0.05 V vs RHE a small dark current of −5 μA.cm^{-2} is observed (Figure 2A). Cyclic voltammetry and emission spectroscopy of **RBG-174** and **CoHEC** in solution indicate that there are significant driving forces for hole injection from the **RBG-174** excited state to **NiO** and for electron transfer from reduced **RBG-174** to **CoHEC** to form Co^{I} (Figure 1, Table S2). Under illumination (800 nm > λ > 400 nm, 50 mW.cm^{-2}) the electrode displays a photocurrent of −12 μA

5

at 0.14 V and the magnitude of additional current due to illumination increases when scanning from anodic to cathodic potential. Following this, chronoamperometry was performed at three different potentials in order to understand the magnitude and stability of dark- and photo-currents at potentials relevant for photo-driven H_2 production (Figure 2B). In all cases, the currents show good stability on the scale of minutes, except for an initial rapid decay after turning on the light. Moving from 0.54 to 0.34 V the dark current increases by -1 $\mu A.cm^{-2}$, but the photocurrent increases by -5 $\mu A.cm^{-2}$. Moving from 0.34 V to 0.14 V vs RHE, there is no change in the dark current and the photocurrent increases again, to a stable -7 $\mu A.cm^{-2}$.
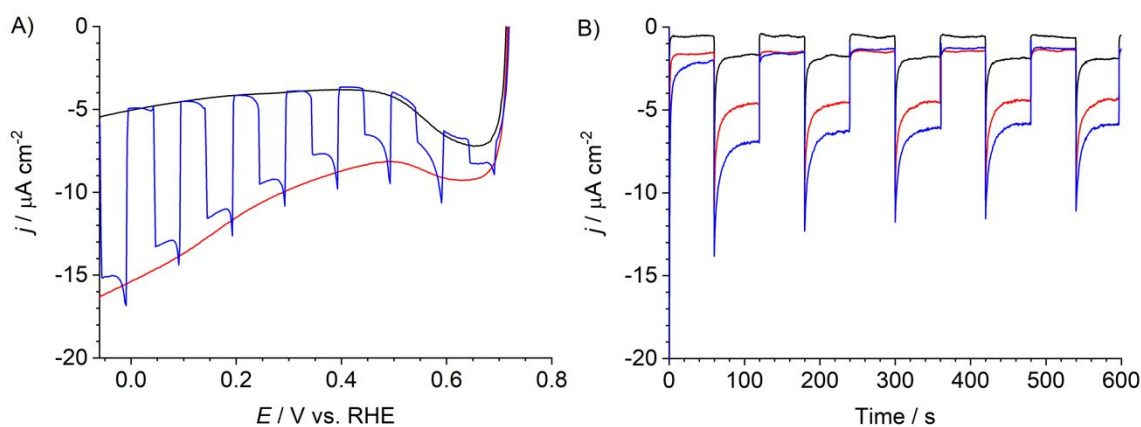

Figure 2. A) LSV of **NiO|RBG-174|CoHEC** without (black) and with (red) illumination (800 nm > λ > 400 nm, 50 mW.cm^{-2}), and under chopped illumination (blue) in MES buffer (0.1 M, pH 5.5). B) Chronoamperometry of **NiO|RBG-174|CoHEC** under chopped illumination (800 nm > λ > 400 nm, 50 mW.cm^{-2}) in MES buffer (0.1 M, pH 5.5) at 0.54 V (black), 0.34 V (red) and 0.14 V (blue) vs RHE.

Chronoamperometry was performed at 0.14 V vs RHE for 2 h under continuous irradiation (example current density vs time curve in Figure S6) and H_2 was produced with a Faradaic efficiency of 70%, this value accounting for H_2 detected in both solution and headspace.[35] A control experiment was performed with **NiO|RBG-174** co-grafted with [4,4'-bipyridine]-2,6-dicarboxylic acid, the ligand of **CoHEC** in the absence of the cobaloxime catalytic core, which produced a trace of H_2 with a Faradaic efficiency of 7% (headspace H_2 only) and much lower photocurrent (Figure S7 and Table S3). This activity in the absence of cobaloxime most probably originates from the formation of catalytically active Ni particles via reduction by the excited **RBG-174** dye of loosely connected NiO particles from the substrate and is consistent with reports of similar organic

6

structures on NiO.[25, 36] Testing in MES buffer allowed us to make a direct comparison with our previously reported systems based on cobalt diimine dioximes and organic dyes on NiO,[9-10, 35] with either covalently bound dyads or co-grafted dye and catalyst. At the same applied potential, this photocathode outperforms these reported systems, which produced H_2 with 9% Faradaic efficiency (headspace H_2 only)[10] and up to 13% Faradaic efficiency (headspace and solution H_2 measured).[9, 35] The preparation method of NiO has a great effect on the performance of the resulting H_2-evolving photocathode.[37] We chose to use a $NiCl_2$-based four-layer spin-coating technique that we have previously reported.[10] That report was shortly followed by work demonstrating that a four-layer spin coated $NiCl_2$/polymer (F68) mixture is superior to a film made by screen printing nanoparticles.[38] In that study the NiO from the spin-coated $NiCl_2$ paste showed an enhanced rate of hole transport, enhanced dye loading and greater transparency. In a separate report on NiO for OLED applications, it was shown that ozone treatment of NiO creates additional NiO(OH) species and improves hole transport.[30] Ozone treatment causes a darkening of the NiO, likely due to oxidation creating additional Ni^{3+} sites.[39] However, over time this color is lost and once a negative potential is applied, the film becomes transparent. In this study, we observed increased H_2 production for O_3 treated NiO photocathodes, likely due to the improved hole transport: **NiO|RBG-174|CoHEC** photoelectrodes that had not been ozone-treated gave Faradaic efficiencies (headspace only) between 7 and 16%, compared with 49% for those with treatment (pH 5.5 MES buffer). A control experiment with the well-established P1 dye in the absence of catalyst produced no H_2 (Table S3) indicating that the enhanced activity after ozone treatment is not due to H_2 production by modified NiO.

We then evaluated the photocathode in sodium phosphate solution (pH 7, 0.05 M), which is a more suitable buffer for water oxidation at a **TaON|CoO$_x$** photoanode (see below). Under these conditions, the **NiO|RBG-174|CoHEC** photocathode produced H_2 with a Faradaic efficiency of 80% (0.14 V vs RHE applied potential for 2 h, Figure S8). Based on the cobalt loading determined by ICP-AES (12 nmol.cm^{-2} for freshly grafted films), the cobalt-based TON achieved during the first hour is 14; this value is however underestimated if the cobalt loading determined after 1 h of photoelectrochemical activity is taken into consideration. ICP-AES measurements indicate a final surface concentration of 2 nmol.cm^{-2}. This loss of Co from the surface is consistent with a cobaloxime linked to the NiO via axial coordination to a pyridine, as observed for cobaloxime-based electrodes operated in the dark.[40-41] Nevertheless, it seems clear that partial leaching does

not significantly impact the photocurrent value, indicating that enough cobaloxime catalysts remain trapped in the mesoporous NiO to sustain catalysis. The TON achieved by each Co-HEC catalysts thus ranges between 84 and 14.

NiO as a transparent p-type semiconductor has been subject to optimization, due in part to the field of p-type dye sensitized solar cells. However, it is still not ideal due to low hole mobility, low permittivity and an absence of hole traps.[37, 42] Due to the flat band potential of NiO (0.72 V vs RHE), there is an excess of driving force for electron transfer to the dye leading to a loss of overall efficiency.[26] Alternative transparent p-type semiconductors include $CuGaO_2$, which displays a more positive flat band potential (1.06 V vs RHE) than NiO.[26] $CuGaO_2$ is more than two orders of magnitude more conducting than NiO and two times more transparent in the visible range.[43] The carrier density of **$CuGaO_2$** is much higher than NiO at 1.7×10^{18} cm^{-3} compared with $< 10^{13}$ cm^{-3} for NiO.[44-45] We therefore decided to test electrodes based on $CuGaO_2$. Linear sweep voltammetry of **$CuGaO_2$|RBG-174|CoHEC** in pH 7 phosphate buffer (Figure 3A and blue traces in Figure 3B) showed photocurrent with ~400 mV more positive onset and ~45 $\mu A.cm^{-2}$ greater magnitude (at 0 V vs RHE) than for NiO. Chronoamperometry over two hours at 0.41 V vs RHE produced 374 nmol of H_2, which rose to 555 nmol after allowing for gas equilibration into the headspace, equal to 74% Faradaic efficiency (Figure 3C). The $CuGaO_2$ photocathode thus produces a similar Faradaic efficiency to the NiO photocathode but at 300 mV less negative applied potential. The enhanced performance is due to $CuGaO_2$ possessing greater conductivity (resulting in four-fold increase in the current density) and a more positive flat band potential than NiO.[26] The driving force for electron transfer from $CuGaO_2$ to the **RBG-174*** (dye excited state) is smaller than from NiO to **RBG-174*** (Table S2) and, as a result, less energy is lost. ICP-AES measurements indicate a cobalt loading of 2.66 $nmol.cm^{-2}$ before photoelectrolysis and 0.34 $nmol.cm^{-2}$ after photoelectrolysis, giving a cobalt-based TON range between 82 and 640 over 2 h.

To confirm the contribution of the **RBG-174** dye to visible light utilization by the photocathode we performed IPCE action spectra of **$CuGaO_2$** and **$CuGaO_2$|RBG-174|CoHEC** (Figure S9). The bare **$CuGaO_2$** has a limited photo-response reaching up to 460 nm. However, the **$CuGaO_2$|RBG-174|CoHEC** is able to utilize photons up to 600 nm, with 4% IPCE at 500 nm where **$CuGaO_2$** shows only 0.1%. The shoulder at 500 nm matches closely with the diffuse-reflectance spectrum of the photocathode (Figure S9) and the adsorption spectrum of **RBG-174** in solution.[9]
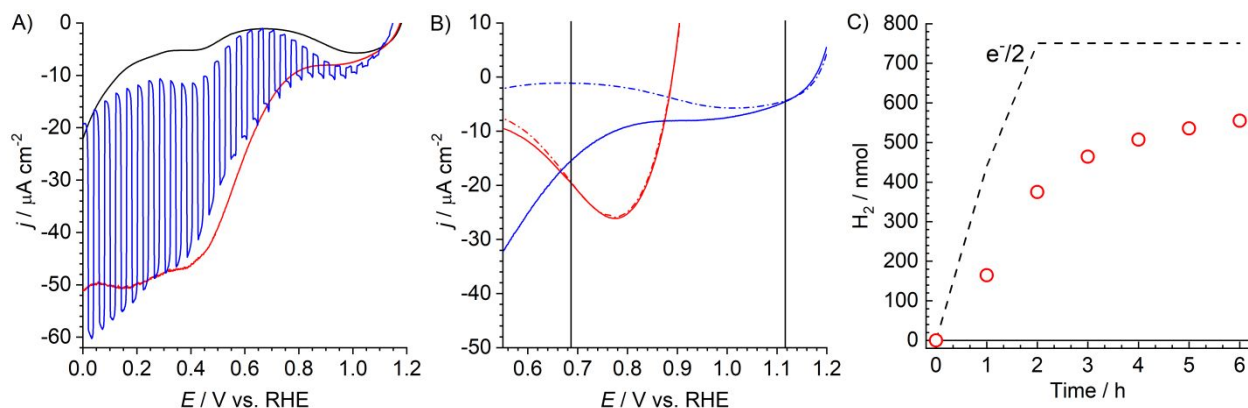
Figure 3. CuGaO₂|RBG-174|CoHEC; A) LSV in the dark (black), with 800 nm > λ > 460 nm (30 mW.cm⁻², red) and chopped 800 nm > λ > 460 nm (30 mW.cm⁻², blue); B) Photocurrent onset **NiO|RBG-174|CoHEC** dark (red dot dash) and 800 nm > λ > 400 nm (50 mW.cm⁻², red solid), **CuGaO₂|RBG-174|CoHEC** dark (blue dot dash) and 800 nm > λ > 460 nm (30 mW.cm⁻², blue solid); C) Chronoamperometry at 0.41 V vs RHE for 2 h (800 nm > λ > 460 nm, 30 mW.cm⁻²) H₂ observed (red circle) and 100% Faradaic yield (black dash). All in 0.05 M sodium phosphate pH 7.

Photoelectrochemical H₂ and O₂ evolution using a Z-scheme configuration

With such an optimized molecular photocathode in hand, we assembled a photocatalytic water splitting Z-scheme device. We selected a photoanode composed of a TaON light-absorbing layer coated with a CoO_x water oxidation catalyst. This electrode is very efficient for water oxidation to O_2, displaying photocurrents of 2 mA.cm⁻² at 1 V vs RHE and splitting water with unity Faradaic efficiency (0.1 M sodium phosphate, pH 8).[46] This photoelectrocatalytic activity (Figure 4) was found unchanged in 0.05 M pH 7 sodium phosphate buffer where a Faradaic efficiency of 97% was measured after gas equilibration into the headspace.
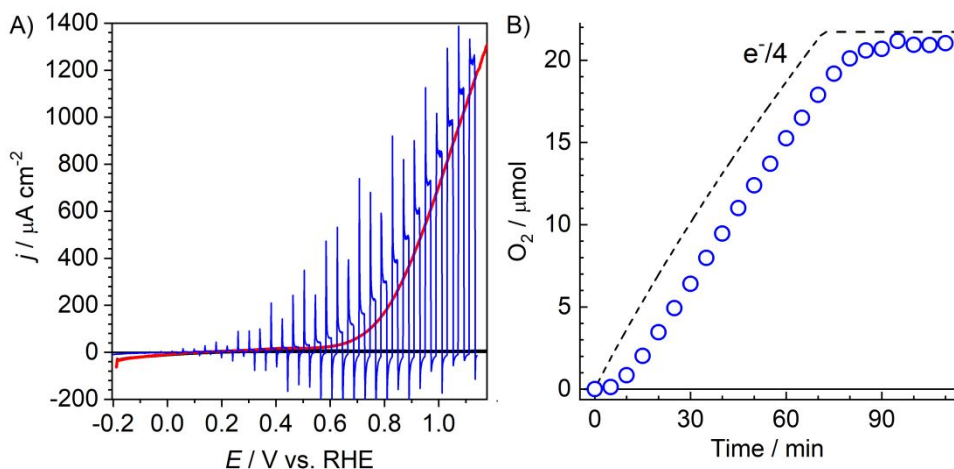
Figure 4. TaON|CoO$_x$ in aqueous sodium phosphate buffer solution (pH 7, 0.05 M) and under irradiation (800 nm > λ > 400 nm, 50 mW.cm^{-2}). A) Current potential curve (irradiation chopped, sweep 10 mV.s^{-1}) B) O$_2$ evolution at 1.07 V vs RHE

Following this, the **CuGaO$_2$|RBG-174|CoHEC** photocathode and the **TaON|CoO$_x$** photoanode were connected in a two-electrode Z-scheme configuration (Figure 5). The complementary visible adsorption profile of the photoelectrodes is demonstrated by the action spectra. The **TaON|CoO$_x$** operates under wavelengths up to 490 nm[47] whereas the **CuGaO$_2$|RBG-174|CoHEC** operates up to 600 nm (Figure S9). The photoelectrodes were installed in two chambers containing pH 7 sodium phosphate buffer that were separated by a Nafion membrane and purged with Ar. The **CuGaO$_2$|RBG-174|CoHEC** photocathode and the **TaON|CoO$_x$** photoanode were irradiated independently with 800 nm> λ > 460 nm (30 mW.cm^{-2}) and 800 nm > λ > 400 nm (50 mW.cm^{-2}), respectively, using appropriate filters and IR-blocking mirrors. The irradiance corresponds to 1 sun, restricted to the visible part of the solar spectrum. Under these conditions, in the absence of any external applied bias, the two-photoelectrode Z-scheme system splits water into H$_2$ and O$_2$. Figure 6C shows time courses for H$_2$ and O$_2$ production. The gases take some minutes to equilibrate from solution to headspace and so two short periods without irradiation allowed for this to take place, resulting in a more accurate evaluation of the photocatalytic activity. After 2 h of irradiation, with an average photocurrent of -10.3 μA (Figure 6B), 294 nmol of H$_2$ and 149 nmol O$_2$ had been produced, corresponding to Faradaic efficiencies of 87% and 88% respectively (Figure 6C). This closely matches the Faradaic efficiencies of the photoelectrodes assessed separately in the three-electrode experiments. Based on the initial and final cobalt loadings, H$_2$ is produced with a TON

range between 44 and 346 over the 2 h period. Throughout photolysis the systems reads a constant working potential of 0.6 V vs RHE, matching the intersection of the photoelectrode current densities which occurs at 0.6 V vs RHE (Figure 6A).
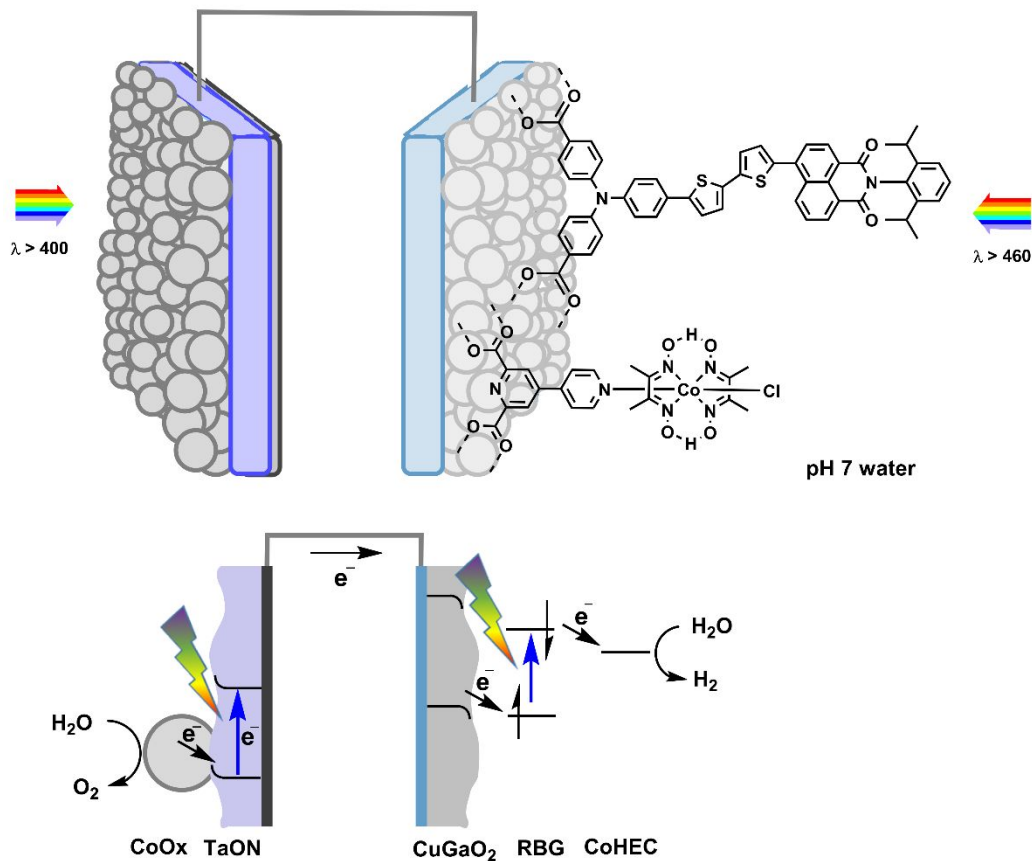

Figure 5. Schematic of the overall water splitting Z-scheme photoelectrochemical cell
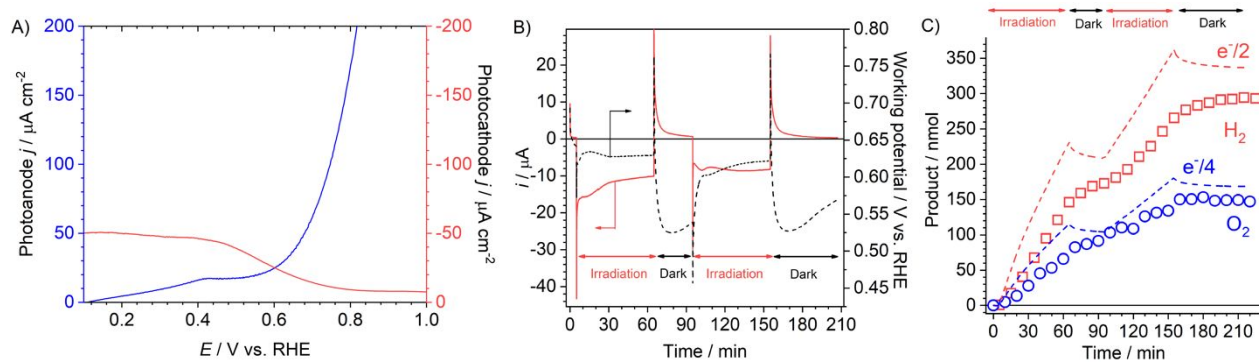
Figure 6. Z-scheme overall water splitting with **CuGaO$_2$|RBG-174|CoHEC** as photocathode (2.3 cm^2) and **TaON|CoO$_x$** as photoanode (2.7 cm^2). A) LSV under irradiation for **CuGaO$_2$|RBG-174|CoHEC** (800 nm > λ > 460 nm, 30 mW.cm^{-2}, red) and **TaON|CoO$_x$** (800 nm > λ > 400 nm, 50 mW.cm^{-2}, blue) B) Current and working potential vs time. C) H$_2$ production (red square) and theoretical H$_2$ production (red dash), O$_2$ production (blue dot) and theoretical O$_2$ production (blue dash).

Using Equation 1 we calculate a solar to hydrogen efficiency of 5.4×10^{-3} % (details in SI).

$$STH = \frac{\text{steady current(mA)} \times \text{Faradaic efficiency (\%)} \times \text{potential (V)}}{\text{total incident light (mW)}} \qquad \text{Equation 1}$$

The Z-Scheme shows good stability on the scale of hours. After an initial decay, the photocurrent remains stable for 2 h (Figure 6B). ICP-AES measurements performed on the photocathode indicate that Co leaches from the electrode surface which may lead to eventual deactivation of the system. While there is little change in photocurrent, the rate of H$_2$ and O$_2$ production slows by the second hour (Figure 6B and C). The photocathode stability is likely to be the limiting component as the photoanode shows excellent stability with steady operation for 24 h.[47] Our device is only the third of such tandem cells (Table 1) and it shows two-times higher photocurrent density as compared with the first reported molecular photoelectrochemical cell.[25,48] It also outperforms the second Z-scheme system that relies on ruthenium as catalyst[24] and for which we could determine an STH of 5.1×10^{-3}% in the steady state (see the supporting information) under more than twice the irradiance compared to our work.[49]

Table 1. Performances of molecular-based Z-scheme overall water splitting photoelectrochemical cells.

	Irradiance (mW.cm^{-2})	Steady current density (μA.cm^{-2})	FY (%)	STH (%)	ref.
NiO|PMI–6T–TPA ‖ BiVO$_4$	-	2	80	-	25
NiO|P1|Co1 ‖ TiO$_2$|L0|Ru1	200	15	55	5.1 × 10^{-3}	24
CuGaO$_2$|RBG-174|CoHEC ‖ TaON|CoO$_x$	80	4.5	87	5.4 × 10^{-3}	this work

In summary, we have presented new molecular photocathodes for H$_2$ production based on a push-pull organic dye and a cobaloxime catalyst. These molecules display 70-80% Faradaic efficiency

on NiO and $CuGaO_2$, the latter showing improved performances in terms of photocurrent values and onset potential because of an improved conductivity and a more positive flat band potential. In combination with a high-performing photoanode for water oxidation, we have created a photoelectrochemical cell that can split water into H_2 and O_2 with 87% and 88% Faradaic efficiency respectively and without any applied bias. This is the highest efficiency reported for a molecular Z-scheme in addition to being noble metal-free.

Moving forward, solar to hydrogen yield must go up and the cost must go down. Noble metals and expensive photovoltaics have already been eliminated. Photocurrent densities must now increase, which can be addressed by improving the nanostructure of the substrate to increase the dye and catalyst loadings, as well as ensuring all photoinduced charges are converted into H_2. This may be achieved by improving charge separation through molecule engineering or gradient doping of materials. Finally, durability must be on the scale of years. At 80%, the Faradaic efficiencies are already high but this might be problematic in the long run if the deviation from 100% is due to self-corrosion of the electrode materials. In the future, we will engineer such systems to protect the electrodes, e.g. through the design of suitable overlayers.

EXPERIMENTAL SECTION

General methods and chemicals used. Isopropanol > 97%, $Na_2HPO_4 \cdot 12H_2O$ > 99%(T), $NaH_2PO_4 \cdot 2H_2O$ 99.0%-102.0%(T), Cu_2O > 92%(T) (Kanto Chemical), Ga_2O_3 99.99+% (Wako Chemical) Chloro([4,4'-bipyridine]-2,6-dicarboxylic acid)bis(dimethylglyoximato)cobalt(III) (**CoHEC**) [4,4'-bipyridine]-2,6-dicarboxylic acid (Dyenamo). RBG-174 was prepared following a literature procedure.[19, 27] All other reagents were obtained from commercially available sources and used without further purification. DMF was purchased anhydrous and dried further with 4Å molecular sieves inside an argon filled glovebox. Chemical reagents were purchased from Sigma-Aldrich and used as received.

General characterization methods and equipment. UV/vis absorption spectra were recorded on an Agilent Technologies Cary 60 UV-Vis spectrometer. X-ray photoelectron spectroscopy (XPS) was measured with a Kratos Analytical Axis Ultra DLD spectrometer, using an Mg Kα source at 1253.6 eV, a hemispheric analyzer working at pass energy of 40 eV was used for core levels spectrum. ICP-AES: samples were prepared by submerging the electrodes in 65% HNO_3 (Chem-Lab Nitric acid 65% (ultra-pure)) and sonicating overnight. The solution was then diluted 6.5× by

the addition of H_2O to give an HNO_3 concentration of 10%. The measured concentration of Co was then multiplied by 6.5 to account for the dilution and then multiplied by the solution volume to give absolute moles of Co. This was then divided by the geometrical area of the electrode to give the Co loading in nmoles per square centimeter. The resulting solutions were then submitted to ICP-AES (Shimadzu ICPE-9000 Plasma Atomic Emission spectrometer, calibrated using commercial standards). Amounts of hydrogen in the solution phase were measured with a Unisense H_2 microsensor in a needle.[35] The amounts of evolved hydrogen in the headspace were determined by sampling aliquots to a Perkin Elmer Clarus 580 gas chromatograph equipped with a molecular sieve 5 Å column (30m – 0.53 mm) and a TCD detector.

Electrochemical and photoelectrochemical measurements.

For NiO photoelectrodes: Electrochemical and photoelectrochemical data were acquired with a Biologic VSP 300 potentiostat. Electrochemical measurements were conducted in a 3-electrode cell. For measurements of compounds in solution the working electrode was glassy carbon. The reference electrode was made of a Ag/AgCl wire dipped into a KCl 3 M solution, separated from the supporting electrolyte by a Vycor® frit, and denoted below as Ag/AgCl. The counter electrode was a Pt wire. For measurements in DMF the supporting electrolyte was $Bu_4N\,PF_6$ (0.1 M). Cyclic voltammograms were typically recorded at a scan rate of 100 mV.s^{-1}. The potential of the reference electrode was calibrated at the beginning and end of each day with ferrocene for organic solvent and K_4FeCN_6 for aqueous. Irradiation was carried out with a 300 W ozone-free Xe lamp (Newport) with a Spectra-Physics 59472 UV cut-off filter (λ < 400 nm) and a water-filled *Spectra-Physics 6123NS* liquid filter for elimination of IR (λ > 800 nm) irradiation. The power density was 50 mW.cm^{-2} calibrated using a Newport 91150V reference cell and meter. The photocurrent measurements were carried out in a specifically designed three-electrode cell, using the NiO-sensitized film as the working electrode, Ag/AgCl as the reference electrode and a Ti wire as the counter electrode. The counter electrode compartment was separated from the cathodic one by a frit. The supporting electrolyte was a 0.1 M 2-(N-morpholino)ethanesulfonic acid (MES)/0.1 M NaCl buffer at pH 5.5. The solution was degassed with nitrogen for 20 minutes prior to use. In a typical experiment, the volume of supporting electrolyte was 4.0 mL and the headspace was 1.3 mL.

The dye loading on NiO was calculated using equation (1):

Surface concentration (mol cm^{-2}) = absorbance/(1000 × ε_{max})   equation 1,

where ε_{max} is the molar absorption coefficient in M^{-1}.cm^{-1}

For RBG on NiO the absorbance at 442 nm was taken from Figure S5 and ε_{max} has been reported.[9]

Our protocol for the quantification of hydrogen by gas chromatography and the Unisense H$_2$ microsensor has been reported in detail.[35] In brief, the GC was calibrated using known concentrations of H$_2$ gas in N$_2$ to create a calibration curve of peak area vs moles of hydrogen injected. Aliquots from the photoelectrochemical cell were injected int the GC. The H$_2$ peak area was integrated and the moles of H$_2$ were calculated using the calibration curve. This was then multiplied by how many times larger the cell headspace is than the syringe volume to give the total moles of H$_2$. The H$_2$ microsensor was calibrated using known concentrations of H$_2$ in electrolyte to give a calibration curve of sensor signal in mV vs H$_2$ concentration. At the end of photoelectrolysis the sensor was inserted into the photoelectrochemical cell. The signal readout was converted to the concentration of H$_2$ using the calibration curve. The H$_2$ concentration was then multiplied by the volume of solution in the cell to give the total moles of H$_2$. The total moles of H$_2$ were converted to Faradaic efficiency using equation (2).

Faradaic efficiency = moles H$_2$ / [(charge passed / F)/2]   equation 2,

where charge passed is in coulombs and F is the Faraday constant in C.mol^{-1}.

For CuGaO$_2$ and TaON|CoO$_x$ photoelectrodes: A three-electrode setup with an HZ-7000 potentiostat (Hokuto Denko) was used throughout the photoelectrochemical measurements and half reactions. A 0.05 M aqueous solution of sodium phosphate (pH 7) was used as electrolyte. A Pt wire and Ag/AgCl in a saturated aqueous solution of KCl were employed as the counter and reference electrodes, respectively. The counter electrode was separated from the reaction solution using a Nafion 117 membrane to avoid the influence of the oxidation reaction taking place on the counter electrode. The working electrode (ca. 2.5 cm^2) was irradiated using a 300 W Xe lamp (Asahi Spectra MAX-302) with an IR-blocking mirror module. Cutoff filters (HOYA Y48 and L42, for irradiation at λ > 460 nm and at λ > 400 nm, respectively) were employed to control the irradiation wavelength. The lamp power was calibrated to 50 mW.cm^{-2}. The potential against a reversible hydrogen electrode (RHE) was calculated using the Nernst equation (equation (3)):

E (V vs. RHE) = E (V vs Ag/AgCl) + 0.199 + 0.059 pH   equation 3

The action spectra of the IPCE were calculated using equation (4):

IPCE (%) = [(1240/λ_{ex})(I_{light} - I_{dark})/P_{light}] × 100   equation 4,

where λ_{ex} and P_{light} are the wavelength and power density of the incident light (nm and mW.cm^{-2}), respectively, (I_{light} is the current density under irradiation (mA.cm^{-2}), and I_{dark} is the current density in the dark (mA.cm^{-2}).

The photoelectrochemical production of H$_2$ was conducted using a Pyrex cell sealed with an O-ring and a stir bar. The headspace volume of the cell was ca. 12 mL, and 15 mL of the electrolyte solution was utilized. The reaction was conducted after purging the system with Ar for more than 20 minutes. A cutoff filter (HOYA Y48) was employed for irradiation at λ > 460 nm. Product analysis of H$_2$ or O$_2$ in the gas phase was performed using in-line gas chromatography (Inficon MGC3000A). The Faradaic efficiency was calculated from the gas chromatography data using the method given above for NiO photoelectrodes.

Z-scheme: The reaction was conducted using a Pyrex cell with two chambers (ca. 27 mL for each chamber) that were divided by a Nafion 117 membrane (Aldrich). The photoelectrodes were fitted into each chamber and the cell was sealed with an O-ring. Ag/AgCl in a saturated aqueous solution of KCl was employed as the reference electrode and was placed into the cathode chamber. A 15 mL portion of a 0.05 M aqueous solution of pH 7 sodium phosphate was added as an electrolyte to each chamber, which was purged with Ar. A three-electrode setup with an HZ-7000 potentiostat (Hokuto Denko) was used in nonresistance ammeter mode. The **CuGaO$_2$|RBG-174|CoHEC** photocathode (ca. 2.3 cm^2) was irradiated at 800 nm > λ > 460 nm using a 300 W Xe lamp (Asahi Spectra MAX-302) with a cutoff filter (HOYA Y48) and an IR-blocking mirror module. The **TaON|CoO$_x$** photoanode (ca. 2.7 cm^2) was irradiated at 800 nm > λ > 400 nm using a 300 W Xe lamp (Asahi Spectra MAX-303) with a cutoff filter (HOYA L42) and an IR-blocking mirror module. The 800 nm > λ > 460 nm intensity at the cathode was set to 30 mW.cm^{-2} and the 800 nm > λ > 400 nm intensity at the anode was set to 50 mW.cm^{-2} so that the light intensities for the wavelengths not blocked by the filters were approximately the same. 50 mW.cm^{-2} for 800 nm > λ > 400 nm also matches the intensities and wavelengths used in the three electrode experiments for NiO and corresponds approximately to 1 sun irradiation in this wavelength range. The analysis

of gas products was performed using in-line gas chromatography (Inficon MGC3000A). The Faradaic efficiency was calculated from the gas chromatography data using the method given above for NiO photoelectrodes.

Preparation of photoelectrodes

NiO: Anhydrous $NiCl_2$ (3g) and F108 (3g) were dissolved in H_2O (9 g) and Ethanol (18 g) and sonicated overnight, followed by centrifugation. The paste was spin coated onto FTO-glass and sintered at 450 °C for 30 minutes. This was repeated four times. The films were treated in an ozone cleaner (Ossila E511) for 10 minutes immediately before immersion in the dye baths. The NiO|RBG-174|CoHEC electrode was prepared by first soaking the NiO in RBG-174 solution (0.5 mM in CH_2Cl_2 for 5 minutes), rinsing with MeOH (5 minutes) and soaking in CoHEC solution (0.7 mM in MeOH overnight).

CuGaO$_2$: The $CuGaO_2$ particles and subsequent electrodes were prepared according to reported procedures.[26] The hybrid molecular photocathode was prepared by soaking the $CuGaO_2$ electrode in a mixed solution of RBG-174 and CoHEC (0.25 mM and 0.35 mM in MeOH, respectively) over 2.5 d.

TaON|CoO$_x$: The TaON|CoO$_x$ photoanodes were prepared according to a reported procedure.[46]

Corresponding Authors
* Vincent Artero; E-mail: vincent.artero@cea.fr
* Osamu Ishitani; E-mail: ishitani@chem.titech.ac.jp
* Ryu Abe; E-mail: ryu-abe@scl.kyoto-u.ac.jp

Author Contributions

Notes

The authors declare no competing financial interest.

REFERENCES

1. Brennaman, M. K.; Dillon, R. J.; Alibabaei, L.; Gish, M. K.; Dares, C. J.; Ashford, D. L.; House, R. L.; Meyer, G. J.; Papanikolas, J. M.; Meyer, T. J., Finding the Way to Solar Fuels with Dye-Sensitized Photoelectrosynthesis Cells. *J. Am. Chem. Soc.* **2016,** *138*, 13085-13102.
2. Bolton, J. R.; Strickler, S. J.; Connolly, J. S., Limiting and realizable efficiencies of solar photolysis of water. *Nature* **1985,** *316*, 495.
3. Ager, J. W.; Shaner, M. R.; Walczak, K. A.; Sharp, I. D.; Ardo, S., Experimental demonstrations of spontaneous, solar-driven photoelectrochemical water splitting. *Energy Environ. Sci.* **2015,** *8*, 2811-2824.
4. Pan, L.; Kim, J. H.; Mayer, M. T.; Son, M.-K.; Ummadisingu, A.; Lee, J. S.; Hagfeldt, A.; Luo, J.; Grätzel, M., Boosting the performance of Cu2O photocathodes for unassisted solar water splitting devices. *Nature Catalysis* **2018,** *1*, 412-420.
5. McKone, J. R.; Lewis, N. S.; Gray, H. B., Will Solar-Driven Water-Splitting Devices See the Light of Day? *Chem. Mater.* **2014,** *26*, 407-414.
6. Leung, J. J.; Warnan, J.; Nam, D. H.; Zhang, J. Z.; Willkomm, J.; Reisner, E., Photoelectrocatalytic H2 evolution in water with molecular catalysts immobilised on p-Si via a stabilising mesoporous TiO2 interlayer. *Chem. Sci.* **2017,** *8*, 5172-5180.
7. Gibson, E. A., Dye-sensitized photocathodes for H-2 evolution. *Chem. Soc. Rev.* **2017,** *46*, 6194-6209.
8. Queyriaux, N.; Kaeffer, N.; Morozan, A.; Chavarot-Kerlidou, M.; Artero, V., Molecular cathode and photocathode materials for hydrogen evolution in photoelectrochemical devices. *J. Photochem. Photobiol. C* **2015,** *25*, 90-105.
9. Kaeffer, N.; Windle, C. D.; Brisse, R.; Gablin, C.; Léonard, D.; Jousselme, B.; Chavarot-Kerlidou, M.; Artero, V., Insights into Mechanism and Aging of a noble-metal free H2-evolving Dye-Sensitized Photocathode. *Chem. Sci.* **2018,** *9*, 6721–6738.
10. Kaeffer, N.; Massin, J.; Lebrun, C.; Renault, O.; Chavarot-Kerlidou, M.; Artero, V., Covalent Design for Dye-Sensitized H2-Evolving Photocathodes Based on a Cobalt Diimine–Dioxime Catalyst. *J. Am. Chem. Soc.* **2016,** *138*, 12308-12311.
11. Gross, M. A.; Creissen, C. E.; Orchard, K. L.; Reisner, E., Photoelectrochemical hydrogen production in water using a layer-by-layer assembly of a Ru dye and Ni catalyst on NiO. *Chem. Sci.* **2016,** *7*, 5537-5546.

12.   Kamire, R. J.; Majewski, M. B.; Hoffeditz, W. L.; Phelan, B. T.; Farha, O. K.; Hupp, J. T.; Wasielewski, M. R., Photodriven hydrogen evolution by molecular catalysts using Al2O3-protected perylene-3,4-dicarboximide on NiO electrodes. *Chem. Sci.* **2017,** *8*, 541-549.

13.   Click, K. A.; Beauchamp, D. R.; Huang, Z.; Chen, W.; Wu, Y., Membrane-Inspired Acidically Stable Dye-Sensitized Photocathode for Solar Fuel Production. *J Am Chem Soc* **2016,** *138*, 1174-9.

14.   Pati, P. B.; Zhang, L.; Philippe, B.; Fernández-Terán, R.; Ahmadi, S.; Tian, L.; Rensmo, H.; Hammarström, L.; Tian, H., Insights into the Mechanism of a Covalently-Linked Organic Dye-Cobaloxime Catalyst System for Dye Sensitized Solar Fuel Devices. *ChemSusChem* **2017,** *10*, 2480–2495.

15.   Brown, A. M.; Antila, L. J.; Mirmohades, M.; Pullen, S.; Ott, S.; Hammarström, L., Ultrafast Electron Transfer Between Dye and Catalyst on a Mesoporous NiO Surface. *J. Am. Chem. Soc.* **2016,** *138*, 8060-8063.

16.   Shan, B.; Das, A. K.; Marquard, S.; Farnum, B. H.; Wang, D.; Bullock, R. M.; Meyer, T. J., Photogeneration of hydrogen from water by a robust dye-sensitized photocathode. *Energy Environ. Sci.* **2016,** *9*, 3693-3697.

17.   Shan, B.; Sherman, B. D.; Klug, C. M.; Nayak, A.; Marquard, S. L.; Liu, Q.; Bullock, R. M.; Meyer, T. J., Modulating Hole Transport in Multilayered Photocathodes with Derivatized p-Type Nickel Oxide and Molecular Assemblies for Solar-Driven Water Splitting. *J. Phys. Chem. Lett.* **2017,** *8*, 4374-4379.

18.   Wang, D.; Sheridan, M. V.; Shan, B.; Farnum, B. H.; Marquard, S. L.; Sherman, B. D.; Eberhart, M. S.; Nayak, A.; Dares, C. J.; Das, A. K.; Bullock, R. M.; Meyer, T. J., Layer-by-Layer Molecular Assemblies for Dye-Sensitized Photoelectrosynthesis Cells Prepared by Atomic Layer Deposition. *J. Am. Chem. Soc.* **2017,** *139*, 14518-14525.

19.   Brisse, R.; Faddoul, R.; Bourgeteau, T.; Tondelier, D.; Leroy, J.; Campidelli, S.; Berthelot, T.; Geffroy, B.; Jousselme, B., Inkjet Printing NiO-Based p-Type Dye-Sensitized Solar Cells. *ACS Appl Mater Interfaces* **2017,** *9*, 2369-2377.

20.   Kaeffer, N.; Morozan, A.; Artero, V., Oxygen Tolerance of a Molecular Engineered Cathode for Hydrogen Evolution Based on a Cobalt Diimine–Dioxime Catalyst. *J. Phys. Chem. B* **2015,** *119*, 13707-13.

21.   Wakerley, D. W.; Reisner, E., Oxygen-tolerant proton reduction catalysis: much O2 about nothing? *Energy Environ. Sci.* **2015,** *8*, 2283-2295.

22.   Yu, Z.; Li, F.; Sun, L., Recent advances in dye-sensitized photoelectrochemical cells for solar hydrogen production based on molecular components. *Energy Environ. Sci.* **2015,** *8*, 760-775.

23.   Xu, P. T.; McCool, N. S.; Mallouk, T. E., Water splitting dye-sensitized solar cells. *Nano Today* **2017,** *14*, 42-58.

24.   Li, F.; Fan, K.; Xu, B.; Gabrielsson, E.; Daniel, Q.; Li, L.; Sun, L., Organic Dye-Sensitized Tandem Photoelectrochemical Cell for Light Driven Total Water Splitting. *J. Am. Chem. Soc.* **2015,** *137*, 9153-9159.

25.   Tong, L.; Iwase, A.; Nattestad, A.; Bach, U.; Weidelener, M.; Gotz, G.; Mishra, A.; Bauerle, P.; Amal, R.; Wallace, G. G.; Mozer, A. J., Sustained solar hydrogen generation using a dye-sensitised NiO photocathode/BiVO4 tandem photo-electrochemical device. *Energy Environ. Sci.* **2012,** *5*, 9472-9475.

26.   Kumagai, H.; Sahara, G.; Maeda, K.; Higashi, M.; Abe, R.; Ishitani, O., Hybrid photocathode consisting of a CuGaO2 p-type semiconductor and a Ru(II)-Re(I) supramolecular

photocatalyst: non-biased visible-light-driven CO2 reduction with water oxidation. *Chem. Sci.* **2017,** *8*, 4242-4249.

27.   Brisse, R.; Praveen, C.; Maffeis, V.; Bourgeteau, T.; Tondelier, D.; Berthelot, T.; Geffroy, B.; Gustavsson, T.; Raimundo, J. M.; Jousselme, B., A red to blue series of push-pull dyes for NiO based p-DSSCs. *Sustain. Energy Fuels* **2018,** *2*, 648-654.

28.   Fan, K.; Li, F.; Wang, L.; Daniel, Q.; Gabrielsson, E.; Sun, L., Pt-free tandem molecular photoelectrochemical cells for water splitting driven by visible light. *Phys. Chem. Chem. Phys.* **2014,** *16*, 25234-25240.

29.   Panagiotopoulos, A.; Ladomenou, K.; Sun, D.; Artero, V.; Coutsolelos, A. G., Photochemical hydrogen production and cobaloximes: the influence of the cobalt axial N-ligand on the system stability. *Dalton Trans.* **2016,** *45*, 6732-6738.

30.   Liu, S.; Liu, R.; Chen, Y.; Ho, S.; Kim, J. H.; So, F., Nickel Oxide Hole Injection/Transport Layers for Efficient Solution-Processed Organic Light-Emitting Diodes. *Chem. Mater.* **2014,** *26*, 4528-4534.

31.   Boschloo, G.; Hagfeldt, A., Spectroelectrochemistry of nanostructured NiO. *J. Phys. Chem. B* **2001,** *105*, 3039-3044.

32.   Muresan, N. M.; Willkomm, J.; Mersch, D.; Vaynzof, Y.; Reisner, E., Immobilization of a Molecular Cobaloxime Catalyst for Hydrogen Evolution on a Mesoporous Metal Oxide Electrode. *Angew. Chem. Int. Ed.* **2012,** *51*, 12749-12753.

33.   Andreiadis, E. S.; Jacques, P. A.; Tran, P. D.; Leyris, A.; Chavarot-Kerlidou, M.; Jousselme, B.; Matheron, M.; Pecaut, J.; Palacin, S.; Fontecave, M.; Artero, V., Molecular engineering of a cobalt-based electrocatalytic nanomaterial for H(2) evolution under fully aqueous conditions. *Nat. Chem.* **2013,** *5*, 48-53.

34.   Natu, G.; Hasin, P.; Huang, Z.; Ji, Z.; He, M.; Wu, Y., Valence band-edge engineering of nickel oxide nanoparticles via cobalt doping for application in p-type dye-sensitized solar cells. *ACS Appl. Mater. Interfaces* **2012,** *4*, 5922-5929.

35.   Windle, C. D.; Massin, J.; Chavarot-Kerlidou, M.; Artero, V., A protocol for quantifying hydrogen evolution by dye-sensitized molecular photocathodes and its implementation for evaluating a new covalent architecture based on an optimized dye-catalyst dyad. *Dalton Trans.* **2018,** *47*, 10509-10516.

36.   Hoogeveen, D. A.; Fournier, M.; Bonke, S. A.; Nattestad, A.; Mishra, A.; Bäuerle, P.; Spiccia, L.; Mozer, A. J.; Simonov, A. N., Origin of Photoelectrochemical Generation of Dihydrogen by a Dye-Sensitized Photocathode without an Intentionally Introduced Catalyst. *J. Phys. Chem. C* **2017,** *121*, 25836-25846.

37.   Wood, C. J.; Summers, G. H.; Clark, C. A.; Kaeffer, N.; Braeutigam, M.; Carbone, L. R.; D'Amario, L.; Fan, K.; Farre, Y.; Narbey, S.; Oswald, F.; Stevens, L. A.; Parmenter, C. D. J.; Fay, M. W.; La Torre, A.; Snape, C. E.; Dietzek, B.; Dini, D.; Hammarstrom, L.; Pellegrin, Y.; Odobel, F.; Sun, L.; Artero, V.; Gibson, E. A., A comprehensive comparison of dye-sensitized NiO photocathodes for solar energy conversion. *Phys. Chem. Chem. Phys.* **2016,** *18*, 10727-10738.

38.   Li, X.; Yu, F.; Stappert, S.; Li, C.; Zhou, Y.; Yu, Y.; Li, X.; Ågren, H.; Hua, J.; Tian, H., Enhanced Photocurrent Density by Spin-Coated NiO Photocathodes for N-Annulated Perylene-Based p-Type Dye-Sensitized Solar Cells. *ACS Appl. Mater. Interfaces* **2016,** *8*, 19393-19401.

39.   Noonuruk, R.; Wongpisutpaisan, N.; Mukdacharoenchai, P.; Techitdheera, W.; Pecharapa, W., Ozone-Induced Optical Density Change of NiO Thin Films and Their Applicability as Neutral Optical Density Filter. *Procedia Engineering* **2011,** *8*, 212-216.

40.   Donck, S.; Fize, J.; Gravel, E.; Doris, E.; Artero, V., Supramolecular assembly of cobaloxime on nanoring-coated carbon nanotubes: addressing the stability of the pyridine-cobalt linkage under hydrogen evolution turnover conditions. *Chem. Commun.* **2016,** *52*, 11783-11786.

41.   Reuillard, B.; Warnan, J.; Leung, J. J.; Wakerley, D. W.; Reisner, E., A Poly(cobaloxime)/Carbon Nanotube Electrode: Freestanding Buckypaper with Polymer-Enhanced H2 -Evolution Performance. *Angew Chem Int Ed Engl* **2016,** *55*, 3952-7.

42.   Odobel, F.; Pellegrin, Y.; Gibson, E. A.; Hagfeldt, A.; Smeigh, A. L.; Hammarstrom, L., Recent advances and future directions to optimize the performances of p-type dye-sensitized solar cells. *Coord. Chem. Rev.* **2012,** *256*, 2414-2423.

43.   Renaud, A.; Chavillon, B.; Le Pleux, L.; Pellegrin, Y.; Blart, E.; Boujtita, M.; Pauporté, T.; Cario, L.; Jobic, S.; Odobel, F., CuGaO2: a promising alternative for NiO in p-type dye solar cells. *J. Mater. Chem.* **2012,** *22*, 14353-14356.

44.   Ueda, K.; Hase, T.; Yanagi, H.; Kawazoe, H.; Hosono, H.; Ohta, H.; Orita, M.; Hirano, M., Epitaxial growth of transparent p-type conducting CuGaO2 thin films on sapphire (001) substrates by pulsed laser deposition. *J. Appl. Phys.* **2001,** *89*, 1790-1793.

45.   Guo, W.; Hui, K. N.; Hui, K. S., High conductivity nickel oxide thin films by a facile sol–gel method. *Mater. Lett.* **2013,** *92*, 291-295.

46.   Higashi, M.; Domen, K.; Abe, R., Highly Stable Water Splitting on Oxynitride TaON Photoanode System under Visible Light Irradiation. *J. Am. Chem. Soc.* **2012,** *134*, 6968-6971.

47.   Gujral, S. S.; Simonov, A. N.; Higashi, M.; Fang, X.-Y.; Abe, R.; Spiccia, L., Highly Dispersed Cobalt Oxide on TaON as Efficient Photoanodes for Long-Term Solar Water Splitting. *ACS Catal.* **2016,** *6*, 3404-3417.

48.   This system did not produce detectable O2 and without the incident light intensity we cannot calculate STH.

49.   Disolved hydrogen was not measured for either our Z-Scheme or ref 44.